PAPER

The comparison between modeling of edge localized modes with a current relaxation model and experiment on EAST

IOP Publishing Plasma Physics and Controlled Fusion
Plasma Phys. Control. Fusion 59 (2017) 085010 (8pp) https://doi.org/10.1088/1361-6587/aa7360

The comparison between modeling of edge localized modes with a current relaxation model and experiment on EAST

J Q Cai[1,2], Y Liang[1,3], J Pearson[3], T Zhang[1], Q Zang[1], M Q Wu[1,2], J Huang[1,2] and EAST Team[1]

[1] Institute of Plasma Physics, Chinese Academy of Sciences, PO Box 1126, Hefei 230031, People's Republic of China
[2] University of Science and Technology of China, Hefei 230026, People's Republic of China
[3] Forschungszentrum Juelich GmbH, Association EURATOM-FZ Juelich, Institut fuer Energieforschung—Plasmaphysik, Trilateral Euregio Cluster, D-52425 Juelich, Germany

E-mail: jqcai@ipp.ac.cn

Received 9 January 2017, revised 8 May 2017
Accepted for publication 16 May 2017
Published 15 June 2017

Abstract

The distinctions of edge localized mode (ELM) frequency distributions between moderate and high edge current density cases were observed on the experiment advanced superconducting tokamak. In this paper, a current relaxation model is applied to explain this new observation. It has been demonstrated that the ELM frequency is very sensitive to the edge current density and the edge safety factor by the model predictions. The results also show that, in the large edge current density case, the ELM frequency is subject to a single-peak distribution; while in the moderate edge current density case, the ELM frequency is subject to a roughly multi-peak distribution.

Keywords: EAST, ELMs, current relaxation model

(Some figures may appear in colour only in the online journal)

1. Introduction

Edge localized modes (ELMs), which occur at the edge of the high confinement mode (H-mode) tokamaks, can cause periodic collapses of the H-mode pedestal [1, 2], and lead to a large amount of heat and particle losses from the plasmas. These heat fluxes, especially caused by the large ELMs, will have detrimental consequences for the plasma-facing components in future high power devices, such as the international tokamak experimental reactor (ITER) [3]. ELM control must be based on the understanding of the basic physics of ELMs, which makes understanding the ELM physics a crucial issue for the ITER design and ITER performance.

At present, it is generally agreed that ELMs originate as ballooning or peeling MHD instabilities, which are driven by the steep edge plasma pressure gradient or the large edge plasma current density, respectively. Type-I ELMs, which cause the largest energy losses, are thought to be the coupling of ballooning mode and peeling mode [2, 4, 5]. Here we introduce an extended current relaxation model, which regards the collapse of ELM as a Taylor relaxation process [6, 7] instead of just following the actual dynamics evolution of an ELM collapse.

This extended model was firstly put forward and formulized in the [8, 9] to predict the magnitude and dominant mode numbers of ELMs, and subsequently, it was improved to be able to predict the ELM frequency by taking into account a simple current diffusion model [10]. The previous results indicate that ELM frequency is very sensitive to the edge current density and the edge safety factor. When a low edge current density is considered in this model, multiple peaks appear in the edge safety factor dependence of ELM frequency, that reminds us of an interesting result on JET: a multi-resonance dependence of the ELM frequency on q_{95} has been observed when a low n (=1, 2) field was applied on JET tokamak [11].

The extended Taylor relaxation model has also been demonstrated to explain the multi-resonance behavior in the

dependence of ELM frequency on the edge safety factor observed on TEXTOR tokamak [10]. Unlike the weak pedestal forming in the limiter H-mode on TEXTOR tokamak, experiment advanced superconducting tokamak (EAST) with a divertor configuration has a stronger pedestal, which indicates a higher edge bootstrap current density and diverse edge current density cases. The more complicated edge current density cases make it urgent to study the ELM frequency characteristics on EAST tokamak.

The purpose of this paper is to develop a better understanding of the effects of the edge current density and the edge safety factor on ELM frequency characteristics on EAST, within the main framework of the current relaxation model. In section 2, the outline of the current relaxation model is given. In section 3, the predictions of ELM frequency dependence on the edge safety factor have been made, and applications of the current relaxation model on EAST tokamak have been demonstrated. Lastly, section 4 is the discussion and conclusion.

2. Current relaxation model formulation

In this chapter, the peeling stability criterion in the cylindrical model during the current relaxation process will be given, and the detailed current relaxation process will be described.

2.1. The determination of final relaxed state

During the Taylor relaxation process, the edge plasma will release the extra magnetic potential energy, with conserving the global helicity and the poloidal flux. Therefore, the determination of the final relaxed state can be converted into a functional extremum problem, meaning to find the minimization of the poloidal potential energy W_θ, subject to the conservation of the global helicity K and the poloidal flux Ψ_θ. The potential energy functional is given as

$$W_\theta - \lambda_1 K - \lambda_2 \Psi_\theta = \int_{r_E}^{a} \left[\frac{r^3}{q^2} - \lambda_1 \frac{r}{q}(r^2 - r_E^2) - \lambda_2 \frac{r}{q} \right] \mathrm{d}r. \tag{1}$$

Here λ_1, λ_2 are the Lagrangian multipliers, q is the safety factor, a is the minor radius (which is also the outer boundary position of the relaxed state) and r_E is the inner boundary position of the relaxed region. The equation that minimizes equation (1) is

$$-2\frac{r^3}{q^3} + \lambda_1 \frac{r}{q^2}(r^2 - r_E^2) + \lambda_2 \frac{r}{q^2} = 0 \tag{2}$$

whose solution is

$$q^f(r) = \frac{2r}{\lambda_1 r + (\lambda_2 - \lambda_1 r_E^2)/r} = \frac{1}{C + D/r^2}. \tag{3}$$

By the relation between the toroidal current density and the safety factor

$$J = \frac{B_0}{\mu_0 R_0} \frac{1}{r} \frac{\mathrm{d}}{\mathrm{d}r} \left(\frac{r^2}{q} \right), \tag{4}$$

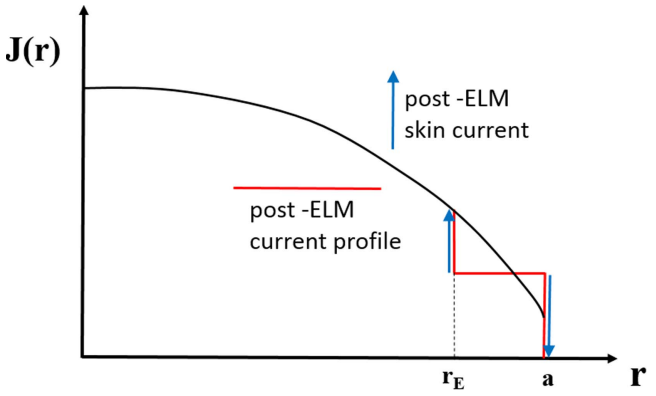

Figure 1. A simple schematic of the current density profile before (black line) and after (red line) ELM. The blue arrow is the skin current formed at the boundaries during the relaxation process.

of which B_0 is the toroidal magnetic field strength, μ_0 is the vacuum permeability and R_0 is the major radius. The corresponding toroidal current density profile of final relaxed state can be derived from equation (3)

$$J^f(\mathrm{r}) = \text{constant} \quad r_E < r < a. \tag{5}$$

The equation (5) indicates that the q profile of the final relaxed state, which has the lowest potential energy, also corresponds to a uniform toroidal current density within the relaxed annulus. It can be found that the edge current density J_a at the final relaxed state exceeds the initial edge current density value in figure 1, which will have a destabilizing effect on the peeling mode. However, an edge negative skin current is formed as the q is discontinuous at the plasma-vacuum interface, which will oppose the rise in J_a and have a counteracting stabilizing effect on peeling mode. Overall, the stabilizing effect dominates the competition, and the peeling mode would be finally stabilized while the relaxation process develops to a certain extent.

Figure 2 shows that the normalized minimum perturbation energy δW of a peeling mode whose poloidal mode number $m = 17$ and toroidal mode number $n = 4$ is negative when the relaxation process just begins ($d_E = 0$), but δW increases subsequently with the increment of d_E and the peeling instability is stabilized at $d_E = 0.132$. The normalized relaxed region width d_E, at which the minimum perturbation energy becomes zero, is termed as the marginal d_E. This model will calculate δW in different modes (m, n), with toroidal numbers increasing from $n = 1$ to $n = 10$ and poloidal mode numbers increasing from $m = nq_a$, which ensures the resonant layer is outside the plasma. Among these values of marginal d_E with different mode numbers, the largest one will determine a state that is stable for all peeling modes. Note that all the peeling modes referred in this paper are external peeling modes since these internal peeling modes are always stable in the relaxed process [9].

2.2. Formulation of the peeling stability criterion

After the final relaxed equilibrium state is established, the next step is to determine the stability criterion in the relaxed state. The peeling stability criterion can be derived from the

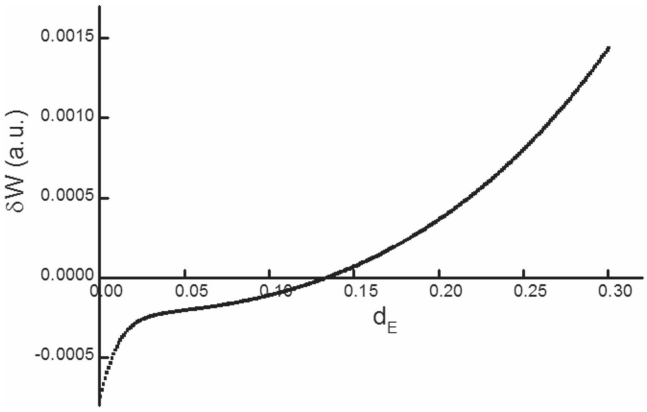

Figure 2. An example of calculating δW with the increment of d_{E}. Here $(m, n) = (17, 4)$ and normalized relaxed region width $d_{\mathrm{E}} = (a - r_{\mathrm{E}})/a$. The condition where $d_{\mathrm{E}} = 0$ indicates the initial condition before the relaxed process and peeling instability is stabilized ($\delta W = 0$) at $d_{\mathrm{E}} = 0.132$.

energy principle, proving the normalized minimum perturbation energy for an ideal MHD cylinder surrounded by vacuum [9, 12, 13] is

$$\delta W = -\Delta_a(\Delta_a\Delta_a' + I_a) - \kappa_a\Big[(\kappa_a - 2\Delta_a) \times (\Delta_a' + m - 1) + 2\frac{n}{m} - I_a\Big]. \quad (6)$$

The four dimensionless quantities used in this model are defined as below:

(a) A dimensionless quantity describing the distance between a radial position j and the resonant surface

$$\Delta_j = \left(\frac{1}{q_j} - \frac{n}{m}\right). \quad (7)$$

Since we consider the external peeling modes, Δ_a would be a small positive real number.

(b) The dimensionless toroidal current density related to the safety factor

$$I_j = \frac{\mu_0 R_0}{B_0} J_j = \frac{1}{r}\frac{\mathrm{d}}{\mathrm{d}r}\left(\frac{r^2}{q_j}\right). \quad (8)$$

(c) The surface current per unit poloidal length

$$\kappa_j = \frac{R_0}{aB_0}\mu_0 J_{js} = \frac{1}{q}\Big|_{j-}^{j+}. \quad (9)$$

(d) The jump in the perturbed poloidal flux radial derivative that is central to the MHD stability analysis:

$$\Delta_j' = \left(\frac{r}{\psi}\frac{\mathrm{d}\psi}{\mathrm{d}r}\right)\Big|_{j-}^{j+}. \quad (10)$$

On the other hand, the stability criterion of the peeling mode in the relaxed state can also be deduced from the basis of marginal force balance in a perturbed plasma. The deducing process is neglected here (the detailed derivation can be found in [9]), and we directly give the stability criterion that the peeling mode will be unstable whenever

$$\Delta_a(\Delta_a\Delta_a' + I_a) + \kappa_a\Big[(\kappa_a - 2\Delta_a)(\Delta_a' + m - 1) + 2\frac{n}{m} - I_a\Big] > 0. \quad (11)$$

Apparently, this criterion is equivalent to the criterion deduced from the energy principle.

2.3. Current relaxation model

The current relaxation process is fully described now: after peeling instability occurs, the edge of plasma will release its excess potential energy to the lowest energy state. This would be achieved by the current relaxation process, which begins from the edge and penetrates into the core. This process will flatten the current density profile in the relaxed region, which has two effects on the peeling mode: destabilizing effect caused by increasing the edge current density, and stabilizing effect contributed by the negative surface current. With the development of the relaxation process, a condition that is stable for all peeling modes can be achieved with a finite d_{E}. Following the relaxation process, flat current density profile starts to diffuse back to the initial current density profile until the next peeling mode is triggered, which initializes a current relaxation process again. That is a continuous ELM cycle.

Since the final relaxed current density profile will diffuse back to the pre-ELM state, an approximation of the ELM frequency can be made by considering the current diffuse time as the ELM repetition time [10, 11]. Here we introduce a simple diffusion model in which D_η is the diffusion coefficient always set to $1\ \mathrm{m^2\,s^{-1}}$ in this model.

$$\frac{\mathrm{d}}{\mathrm{d}t} = D_\eta\frac{\mathrm{d}^2}{\mathrm{d}r^2} \rightarrow f \approx \frac{D_\eta}{d_{\mathrm{E}}^2}. \quad (12)$$

As this model is not aimed to give a quantitative ELM frequency, the value of current diffusion coefficient will not affect the study on characteristics of ELM frequency distribution later.

3. The model predictions and applications on EAST

3.1. The predictions of current relaxation mode

As the equations describing the current relaxation process are established, the main concern now is the program with the aim of investigating the ELM frequency dependence on the edge safety factor in different edge current density cases. The equation (6) describes the normalized minimum perturbation energy with different modes (m, n), and for a given initial q profile and a given mode number (m, n), the minimum

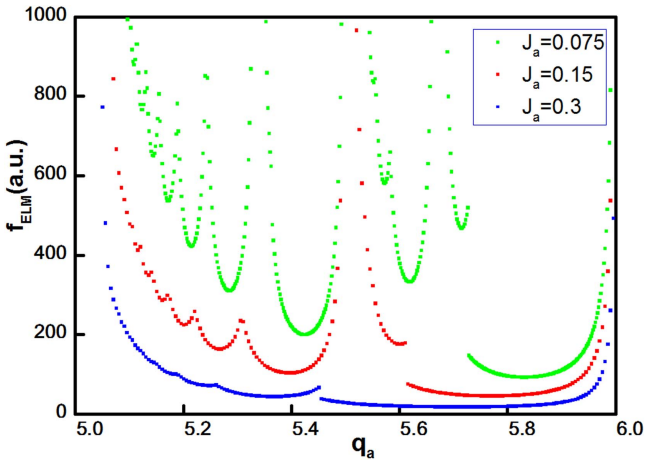

Figure 3. Three plots by the model predictions of f_{ELM} with varying J_a (the normalized current density $J_a = \frac{J_\alpha}{J_0}$), showing the multi-resonance effect increase slowly as J_a decreases. For the convenience of later work, we make a definition: (a) $J_a < 0.1$, a low edge current density case corresponds to a strong multi-resonance effect; (b) $0.1 < J_a < 0.25$, a moderate edge current density case corresponds to a weak multi-resonance effect; (c) $J_a > 0.25$, a high edge current density case corresponds to no multi-resonance effect.

perturbation energy is evaluated as a function of the normalized relaxed region width d_{E}. By inputting the initial edge safety factor and the initial normalized edge current density J_a, predictions can be made of the dominant ELM toroidal and poloidal mode number (m, n) and the relaxed width d_{E}, thus the ELM frequency can be approximately calculated by the diffusion equation (12).

The dependence of the ELM frequency on q_a in different current density cases has been given in figure 3. Multiple strong increase in ELM frequency with the different resonant q_a values in the low edge current density case has been found, which is termed as the multi-resonance effect [11]. Another phenomenon is observed that when the edge current density becomes lower, the multi-resonance effect is stronger. This can be explained by the peeling mode stability criterion in equation (6): when the edge current density is strong enough, I_a dominates the first term in equation (6) resulting in the weak dependence of ELM frequency (more specifically, d_{E}) on q_a; when the edge current density decreases, the effect of term Δ_a which contains q_a becomes dominant. As a consequence, a strong dependence of ELM frequency on q_a can be found.

3.2. The ELM frequency distribution on EAST

Since the edge bootstrap current is the major component of the edge plasma current, the edge current density is roughly equal to the edge bootstrap current density. In the simulation, an approximation of the bootstrap current density can be made with the Sauter model [14] by ONETWO code [15] on EAST. The effective nuclear charge Z_{eff} is set to be 2.5 on EAST, and the edge bootstrap current density can be calculated after obtaining the electron density profile and the electron temperature profile. There are no diagnostics to give a reliable ion temperature profile on this EAST campaign. Due to the high pedestal collisionality in EAST H-mode plasma, we assume that the ion temperature at pedestal is similar to the electron temperature because of the sufficient heat exchange. Besides, the weight coefficient of the bootstrap current contributed by the ion temperature gradient is estimated to be around 0.13 [14], so we have reason to believe that this assumption is reasonable.

To study the ELM frequency dependence on the edge safety factor in different edge current density cases on EAST, electron temperature profiles and density profiles in shots #48059 and #48914 are applied in the bootstrap current density calculation. The parameters of these two shots are as follows: the parameters in #48059 are toroidal field $B_{\mathrm{t}} = 1.85\,\mathrm{T}$, plasma current $I_{\mathrm{p}} = 400\,\mathrm{kA}$, elongation $\kappa = 1.68$, top triangularity $\delta_{\mathrm{top}} = 0.28$ and bottom triangularity $\delta_{\mathrm{bottom}} = 0.56$, while the parameters in #48914 are $B_{\mathrm{t}} = 2.30\,\mathrm{T}$, $I_{\mathrm{p}} = 450\,\mathrm{kA}$, $\kappa = 1.69$, $\delta_{\mathrm{top}} = 0.34$ and $\delta_{\mathrm{bottom}} = 0.59$. Besides, the plasma in #48059 is heated by the neutral beam injection with a power of 3.1 MW, while the plasma in #48914 is heated by the neutral beam injection whose power is 4.5 MW and by the low hybrid wave whose power is 1.7 MW.

The density profiles measured by TS and reflectometry are well aligned, as shown in figure 4, while the density profiles measured by reflectometry are chosen to do the fitting due to its higher spatial resolution and precision. All these profiles are obtained just before the ELM collapse, which indicates that the initial edge current density J_a could be calculated by these profiles.

As shown in figure 5, the bootstrap current density is mainly localized at the plasma edge due to its high pedestal gradient, which gives edge bootstrap current density $340\,\mathrm{kA\,m^{-2}}$ for #48914 and $150\,\mathrm{kA\,m^{-2}}$ for #48059. The toroidal current density profile is reconstructed using equilibrium fitting code [16], and it gives the core current density $950\,\mathrm{kA\,m^{-2}}$ for # 48914 and $800\,\mathrm{kA\,m^{-2}}$ for #48059. Now normalized edge current density $J_a = 0.35$ and $J_a = 0.19$ can be obtained, corresponding to the large edge current density case and the moderate edge current density case for EAST shot #48914 and EAST shot #48059, respectively.

After substituting the normalized edge current density of these two shots into this model, the prediction of ELM frequency on the edge safety factor could be given in figure 6. The shot #48059 corresponds to a weak resonant effect case, while another shows little resonant effect, which makes it interesting to study the distinctions of ELM frequency distributions in these two shots, as shown in figure 8.

The deduction of the peeling stability criterion in this paper is based on a cylindrical approximation, and an issue arises when this model is used in the tokamak with a separatrix geometry. By regarding q_{95} as the effective edge safety factor instead of q_a, some qualitative aspects of the multi-resonance effect on JET [10, 11] could be reproduced in this model. EAST is the first fully superconducting tokamak with

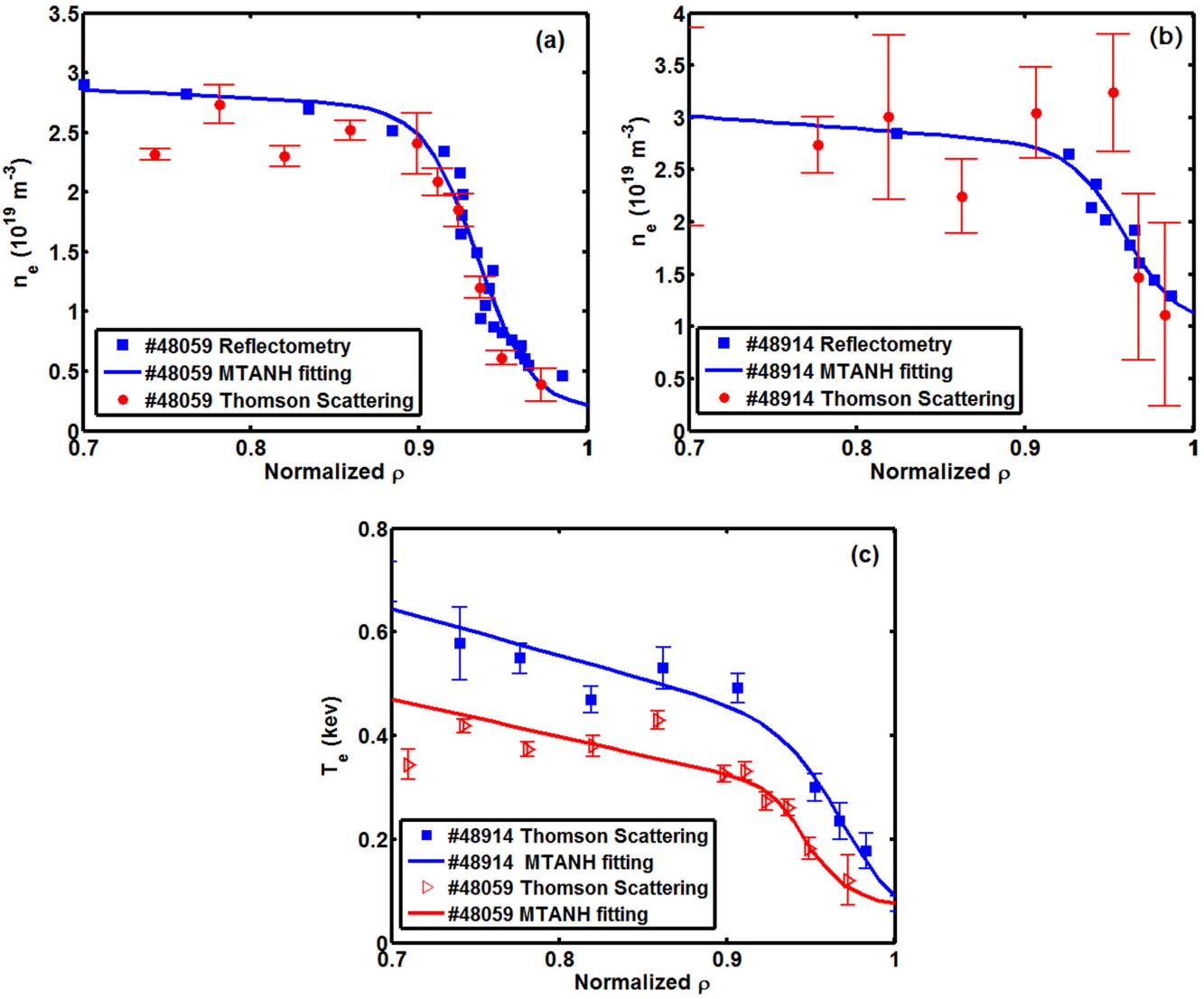

Figure 4. The electron density profile (a) for #48059 and (b) for #48914. The data measured by reflectometry is in blue rectangles while the data measured by Thomson scattering (TS) is in red cycles; the electron temperature profile (c) measured by Thomson scattering (TS) is shown in red triangles for shot #48059 and in blue rectangles for #48914. Here these profiles are all mapped onto normalized poloidal flux surface in which $\rho^*=\sqrt{\frac{\psi_\theta}{\pi B_0}}$. A hyperbolic tangent function (tanh) in the pedestal region has been used to fit these profiles.

advanced divertor configuration, which indicates that the safety factor tends to be infinity at the separatrix. In order to give a qualitative dependence of the ELM frequency distribution on the edge current density, q_{95} is used in this model to replace q_a. However, we should bear in mind that can a full quantitative prediction be given only when the toroidal separatrix geometry has been considered in this model.

The edge safety factor scans were made by varying plasma current I_p on JET [11] and on TEXTOR [10] while keeping toroidal field constant, and the resonant effect has been observed while the edge safety factor meets the resonant value during the scans. In the low edge current density case, a minor variation of edge safety factor would greatly influence the ELM frequency because of the strong resonant effect. Considering the contribution of the toroidal current fluctuations, a minor variation may occur in the safety factor.

The distribution of 2200 toroidal current data from 4.2 to 6.4 s in EAST shot #51016 is shown in figure 7, which are measured by the Rogowski coils [17], obviously indicating that it follows a Gaussian distribution. Similar Gaussian distributions N (402, 2.45) and N (451, 2.2) have also been observed in #48059 and #48914, respectively, with the ratio of standard deviation to expectation being 0.4%–0.6%. Since q_{95} is in reverse proportional to the plasma current, a similar Gaussian distribution could also be used to describe the distribution of q_{95} in these two shots.

In this paper, it is not aimed to give the quantitative ELM frequency, but to study the characteristics of ELM frequency distribution, especially the distinctions of ELM frequency distributions caused by the Gaussian distribution of q_{95} in the different edge current density cases. In order to give a qualitative distribution of ELM frequency, a q_{95} distribution that

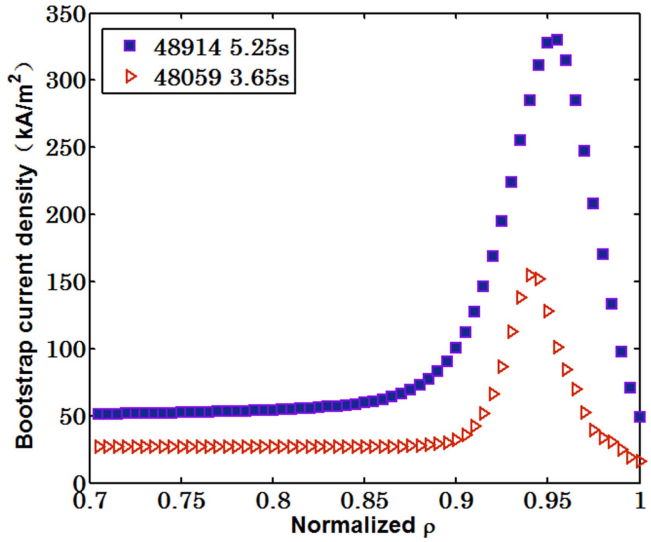

Figure 5. The bootstrap current density profile calculated by ONETWO. EAST shot #48059 is shown in red triangles and EAST shot #48914 is shown in blue rectangles.

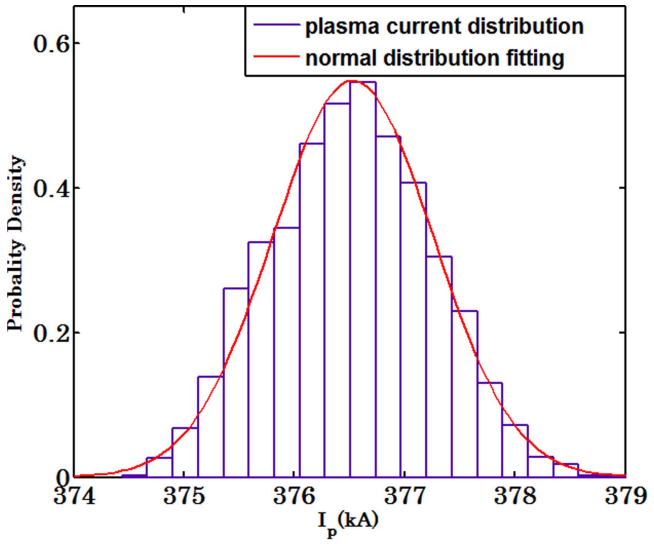

Figure 7. The figure shows the toroidal current distribution diagram of 2200 data from 4.2 to 6.4 s for EAST shot # 51016.

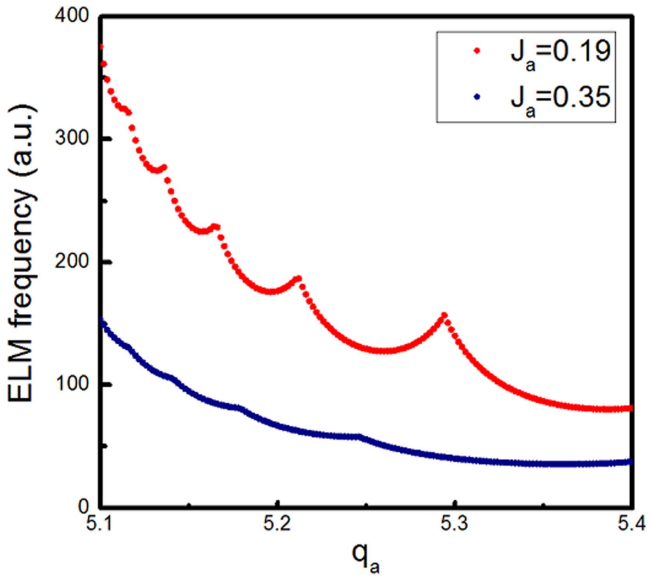

Figure 6. The ELM frequency dependence on the edge safety factor predicted by the model, considering the value of the edge current density on EAST shot #48059 (red) and EAST shot #48914 (blue).

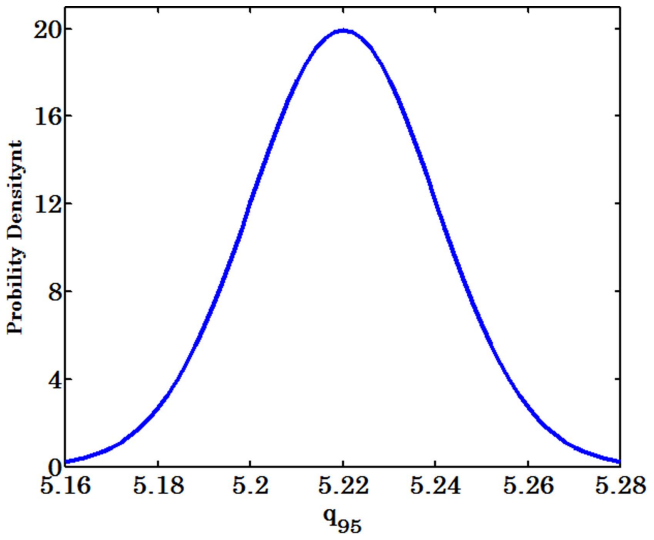

Figure 8. The assumed Gaussian distribution of $q_{95} \sim N$ (5.22, 0.02) in this model.

is subject to N (5.22, 0.02) has been substituted into the current relaxation model. The mainly reason to choose this distribution is that the multi-resonance effect could be better studied as the distribution can span 4 resonant peaks in the moderate edge current density case, as shown in figure 6.

After substituting the assumed q_{95} distribution into the current relaxation model, the distributions of the ELM frequency can be obtained. As figure 9 shows, in the high edge current case ($J_a = 0.35$) the prediction demonstrates a single-peak distribution in which the ELM frequency is localized at around a main frequency; in the moderate edge current case ($J_a = 0.19$), the ELM frequency shows a multi-peak distribution, that is mainly because of the resonance effect of the ELM frequency on q_{95}. This resonance will result in the situation that the ELM frequency near the resonant peaks corresponds to multiple probability density values. When these probability density values are added up, these peaks appear. There exist four frequency peaks, corresponding to the fact that there are four resonant peaks when varying q_{95} from 5.16 to 5.28 in figure 6.

If the Gaussian distribution N (5.22, 0.02) is replaced with different forms like N (4.5, 0.02) or some others, here comes the question that whether there would be any changes in the ELM frequency distribution predicted by the model. In the high edge current density case, the frequency distribution is always subject to a single-peak distribution in whichever

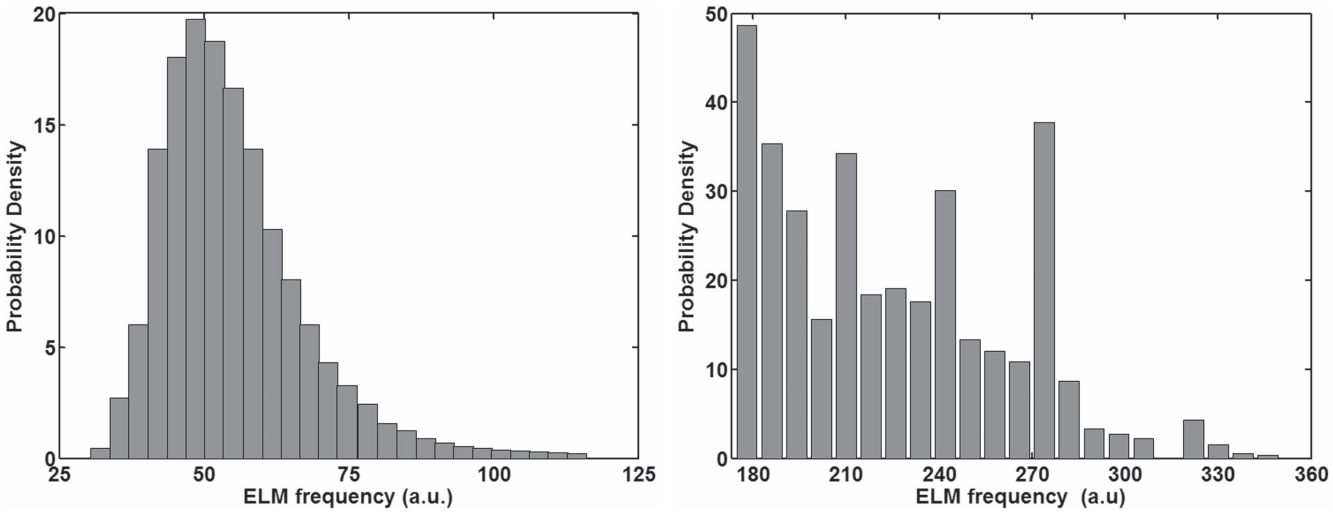

Figure 9. The ELM frequency probability distribution predicted by the model for EAST shot #48914 with $J_a = 0.35$ (left) and EAST shot #48059 with $J_a = 0.19$ (right).

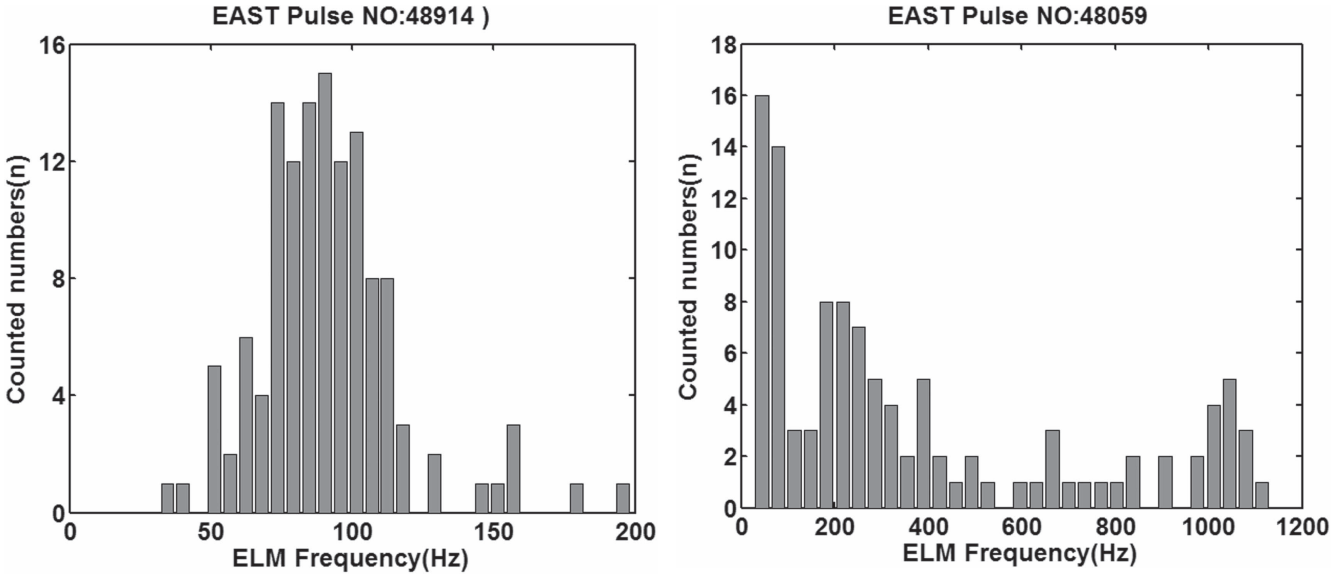

Figure 10. ELM frequency distribution for EAST shot #48914 (left) and EAST shot #48059 (right). When the counted numbers of ELM are large enough, we could think the counted number is a reflection of probability density.

form of Gaussian distribution has been used. While in the low or moderate edge current density case, the number of resonant peaks the Gaussian distribution spans is one important factor in determining the shape of ELM frequency distribution. In most of the case, it would follow a multi-peak distribution.

For comparison, the ELM frequency distributions observed in EAST experiment have also been investigated. Figure 10 shows that the ELM frequency in #48914 focuses around 100 Hz, subject to a single-peak distribution, which is consisted with the model predictions in the high edge current density case. On the other hand, the ELM frequency in #48059 is not subject to a single-peak distribution anymore, although not so obviously, a frequency peak below 100 Hz and another peak near 200 Hz can also be roughly observed.

4. Discussion and conclusion

The differences between ELM frequency distribution in both high and moderate edge current density cases have been studied on EAST, which can be well explained by the current relaxation model. In this model, the role of the bootstrap current is only contributed as the major component of the edge current, and a conventional parabolic current density profile is assumed. The effect of the bootstrap current density profile has not been taken into account in the present model.

The multi-resonance dependence of ELM frequency on the edge safety factor has also been seen in a limiter H-mode plasma on TEXTOR, in which the normalized edge current is only ~0.01 [10], and in the ELM mitigation experiments with $n = 1$ or 2 magnetic perturbations on JET [11]. On EAST, the

effects of edge current density on the ELM frequency distribution have been determined.

In conclusion, a current relaxation model has been applied to predict the ELM frequency distribution on EAST by combining a Gaussian distribution of q_{95}. It has been demonstrated that the ELM frequency is very sensitive to the edge current density and the edge safety factor by the model predictions. In the high edge current density case, the ELM frequency shows a single-peak distribution. In the moderate and low edge current density case, the ELM frequency distribution shows a multi-peak distribution, which may be caused by the multi-resonance effect.

Acknowledgments

This work is supported by the National Magnetic Confinement Fusion Science Program of China under Grant No. 2013GB106003B. The views and opinion expressed herein do not necessarily reflect those of the National Magnetic Confinement Fusion Science Program of China.

References

[1] Zohm H 1996 *Plasma Phys. Control. Fusion* **38** 105
[2] Connor J W 1998 *Plasma Phys. Control. Fusion* **40** 191
[3] Aymar R 2001 *Nucl. Fusion* **41** 1301
[4] Snyder P B *et al* 2002 *Phys. Plasmas* **9** 2037
[5] Connor J W 2008 *AIP Conf. Proc.* **1013** 174
[6] Taylor J B 1974 *Phys. Rev. Lett.* **33** 1139
[7] Taylor J B 1986 *Rev. Mod. Phys.* **58** 741–63
[8] Gimblett C G 2006 *Phys. Rev. Lett.* **96** 035006
[9] Gimblett C G 2006 *Plasma Phys. Control. Fusion* **48** 1531–50
[10] Pearson J 2012 *Nucl. Fusion* **52** 074011
[11] Liang Y 2010 *Phys. Rev. Lett.* **105** 065001
[12] Freidberg J P 1987 *Ideal Magnetohydrodynamics* (New York, London: Plenum)
[13] Bernstein I B, Frieman E A, Kruskal M D and Kulsrud R M 1958 *Proc. R. Soc.* A **244** 17
[14] Sauter O, Angioni C and Lin-Liu Y R 1999 *Phys. Plasmas* **6** 2834
[15] John H St 2005 *Equations and Associated Definitions Used in ONETWO* (https://fusion.gat.com/THEORY/onetwo/)
[16] Liu H Q 2016 *Rev. Sci. Instrum.* **87** 11D903
[17] Chen D L 2015 *Rev. Sci. Instrum.* **86** 103506